The Pennsylvania State University

The Graduate School

Eberly College of Science

EXAMINING THE SURFACE CHEMISTRY AND BEHAVIOR OF COLLOIDALLY-SYNTHESIZED VANADIUM DIOXIDE

A Thesis in

Chemistry

by

Margeaux G. Bull

Submitted in Partial Fulfillment
of the Requirements
for the Degree of

Master of Science

December 2018

The thesis of Margeaux G. Bull was reviewed and approved* by the following:

Raymond E. Schaak
DuPont Professor of Materials Chemistry
Thesis Advisor

Thomas E. Mallouk
Evan Pugh University Professor of Chemistry, Biochemistry and Molecular Biology, Physics, and Engineering Science and Mechanics

Philip C. Bevilacqua
Distinguished Professor of Chemistry and Biochemistry and Biology
Head of the Department of Chemistry

*Signatures are on file in the Graduate School.

Abstract

Since its discovery in the 1960's, vanadium dioxide (VO_2) has been an invaluable compound in research and industry. Due to its unique insulator-metal transition that occurs near room temperature, and its ability to transmit or reflect infrared wavelengths depending on the crystal phase, VO_2 has many possible applications, varying from medical and industrial to military and defense use. One example of an application for VO_2 is its use in metamaterials, which can be designed to manipulate waves of light and sound at the sub-wavelength scale to yield properties not found in nature. Through the use of VO_2, these materials are able to have a tunable response by transmitting or reflecting infrared light, which can be activated by various methods, such as mechanical strain, current, heat, or an applied voltage.

As these metamaterials must be carefully designed and are oftentimes in the nanometer size scale, traditional methods of synthesis, such as chemical vapor deposition and solvothermal synthesis, often do not offer enough control over the size and dispersity of the resulting VO_2 nanoparticles. Instead, colloidal synthesis of VO_2 results in sub-10 nm particles that are relatively monodisperse. However, the colloidal synthesis of VO_2 has not been studied nearly as much as the other synthesis methods. In the research reported herein, VO_2 nanoparticles were colloidally synthesized and characterized, and used in subsequent experiments that involved examining the surface chemistry of the VO_2 to silica coat the particles and form electrostatically-stabilized thin films on metadevice substrates. My research suggests that the colloidally-synthesized VO_2 does not have the same properties as VO_2 synthesized by chemical vapor deposition or solvothermal methods.

Table of Contents

List of Figures

List of Abbreviations

APTMS ([3-aminopropyl]trimethoxysilane)

CTAB (hexadecyltrimethylammonium bromide)

CVD (chemical vapor deposition)

DSC (differential scanning calorimetry)

IMT (insulator-metal transition)

M1 (monoclinic phase)

$NOBF_4$ (nitrosonium tetrafluoroborate)

R (tetragonal, rutile-like phase)

TEM (transmission electron microscopy)

TEOS (tetraethyl orthosilicate)

VO_2 (vanadium dioxide)

XRD (X-ray diffraction)

Acknowledgements

I would first like to thank my research advisor, Dr. Raymond Schaak, for his guidance during my graduate career and support while considering different career options. I would also like to thank my committee member Dr. Thomas Mallouk, as well as Dr. Christine Keating and Dr. Douglas Werner for their help and advice.

I would also like to thank Dr. Nathan Burrows and Dr. Lei Kang for their assistance and advice throughout the research process, as without their insight and expertise, much of this research would not have been possible.

Additionally, I would like to thank the members of the Schaak group for their advice and support throughout my two-and-a-half years here at Penn State. I have not had the smoothest graduate school experience, but you helped make daily life in the Schaak lab more enjoyable. In particular, I would like to thank Xuefei Li for taking me under her wing as I began the vanadium dioxide project, and Dr. Jared Mondschein for supporting me throughout my research experience and while I was debating career decisions.

Lastly, I would like to thank my parents, Deborah Butcher and Scott Bull, and my closest friends, Taylor Harned and Lauren Monce. Graduate school has involved blood, sweat, and tears, and without your love and support (and willingness to answer the phone at any given hour), I would never have made it to where I am now. I know that no matter where life takes me, I will always have you all by my side and will be able to weather any storm.

CHAPTER 1. INTRODUCTION

Introduction to Metamaterials

In the year 2000, Sir John Pendry published his research on the "perfect lens,"[1] which allows for bypassing an important limitation of conventional lenses, which is that they cannot focus light onto an area less than a square wavelength. This was the first concrete example of metamaterials, and since then, the field has greatly expanded. Metamaterials work in a unique way, in that they can manipulate electromagnetic radiation or acoustic waves at sub-wavelength scales. This manipulation allows for the engineering of novel optical and acoustic properties and the control of wave/matter interaction in ways that are not found naturally, through the synthesis of materials designed from sub-wavelength structures. The discovery of metamaterials has led to engineering breakthroughs, such as invisibility cloaks – which have, for example, been active acoustically[2] and at microwave frequencies.[3] These metamaterials offer a wide variety of potential applications in the military and in defense, as well as the industrial and medical fields[4].

One limitation of many metamaterials is that their responses are fixed and not tunable or switchable.[3, 5, 6] In order to enable response modulation of these nanostructured systems to external stimuli, active compounds can be introduced. A popular material used to enable active electromagnetic and optical metadevices is vanadium dioxide (VO_2),[7-10] which undergoes an insulator-metal transition. In the insulating state, VO_2 transmits mid-infrared wavelengths. However, upon transition to the metallic state, it reflects mid-infrared wavelengths. A recent nanophotonic metadevice proved it was possible to "tune" the transmittance and reflectance in the mid-infrared region by introducing the active compound VO_2. In this metadevice, the active

VO_2 layer was incorporated into an optical metamaterial absorber, allowing electrically triggered control in the mid-infrared wavelengths.[11]

VO_2 and its Reversible Insulator-Metal Transition (IMT)

The reversible insulator-metal transition in VO_2 was first discovered in 1959, by F. J. Morin.[12] Since then, the system has since been studied in great depth and become a model system for understanding the role of electron-phonon and electron-electron interactions that affect the magnetic and transport properties of the material.[13, 14]

The IMT in VO_2 can be induced by external stimuli in various ways, such as mechanical strain,[15, 16] heat,[12] and electric field.[17-19] In addition to the many methods of inducing the IMT, VO_2 also offers many possibilities for engineering novel materials, given its near-ambient transition temperature of 340K (68°C), the insulating phase's small band gap of 0.5-0.6 eV,[20] and the ability to control particle size and introduce dopants and lattice strain to affect the phase transition.

Of the known materials with an IMT, the VO_2 phase transition temperature is closest to room temperature,[12] which has led to its popularity and use in the engineering of smart windows,[21, 22] optical switches,[23, 24] memory devices,[25, 26] and Mott transistors.[27, 28] During the insulator to metal phase transition, VO_2 goes from a semiconducting monoclinic (M1) crystal phase to a metallic tetragonal (R) crystal phase.[29]

There are two aspects to this transition – a structural transformation from a low-symmetry, low-temperature phase to a higher-symmetry, high temperature phase, along with an electronic transition from the insulator/semiconducting phase to a metallic phase. Below the transition temperature of 340K, VO_2 crystallizes in its M1 phase (space group $P2_1/c$). In this M1 phase, the vanadium atoms along the c-axis are dimerized and result in two V-V atom

distances, 2.60 Å and 3.19 Å.[30] In addition to the V-V dimerization, the VO_6 octahedra are tilted and distorted. However, upon reaching 340K, a structural transformation occurs and VO_2 adopts the R phase (space group $P4_2/mnm$) with V-V atom distances of 2.85 Å.[30, 31] This structural transition also results in a shift in the lattice parameters, from a = 5.743 Å, b = 4.517 Å, c = 5.375 Å, and ß = 122.61° in the M1 phase, to a/b = 4.555 Å, c = 2.851 Å and ß = 90°, in the R phase (Figure 1).[32] The transition from the insulating monoclinic to the metallic rutile phase results in increased symmetry, as well as a disruption of the V-V dimerization and a straightening of the VO_6 octahedra.[33]

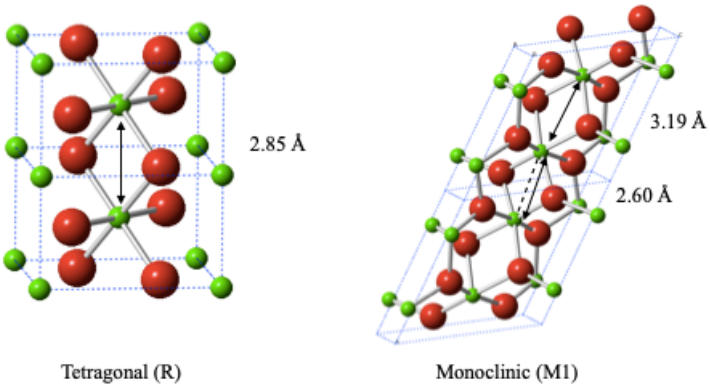

Figure 1. The two crystal phases of vanadium dioxide, tetragonal (left) and monoclinic (right), showing the different V-V atom distances. The vanadium cations are green and the oxygen anions are red.

The structural transition in VO_2 is accompanied by an electronic transition from the insulating phase to the conducting, metallic phase. In the band structure of VO_2, two molecular orbitals are involved in the insulator to metal transition – the V_d d_{II} and V_d-O_p π^*.[29] During this transition, the formation and breaking of V-V bonds and tilting of the VO_6 octahedra aid in the electronic transition process. In the insulating M1 phase, V-V bonds exist, as a result of the V_d d_{II} orbitals, which are directed toward neighboring V atoms, being split into a bonding and antibonding orbital about the fermi level. In addition, the π overlap between the V t_{2g} and O 2p levels is better prior to the VO_6 octahedra tilting, which results in a raised π* antibonding orbital

above the fermi level, due to the stabilized nature of the π overlap. However, upon transition to the R phase, the V-V bonds are broken and the π overlap decreases, due to the VO_6 octahedra straightening throughout the VO_2 crystal structure. This affects the band structure by collapsing the d_{II} bonding and antibonding levels together and lowering the π* antibonding orbital so that they are overlapping with the Fermi level, resulting in a completed transition to the metallic state (Figure 2).[34] It has been proven that the structural and electronic transitions of VO_2 can be decoupled,[13] allowing further insight into the mechanism of transition from the insulating, monoclinic phase to the metallic, rutile phase and how the VO_2 IMT can be controlled for the engineering of novel materials and devices.[35]

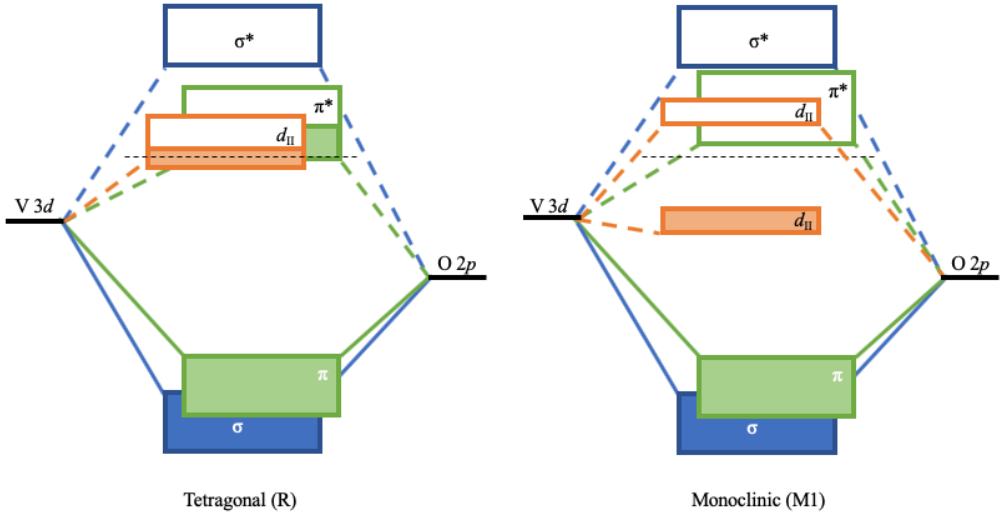

Figure 2. The band diagrams for the tetragonal (R) phase (left) and monoclinic (M1) phase (right). The d_{II} and π orbitals are directly affected by the electronic transition from the metallic phase to the insulating phase.*

Characterization of the IMT

The insulator-metal transition in VO_2 results in two changes in the material's properties in a matter of sub-picoseconds– the first being a large change in resistivity and the second being a transition from infrared-transmitting to infrared-reflecting.[36] The IMT can be characterized

directly, as in bulk or nano-sized VO_2 particles, or indirectly, by measuring the properties exhibited by metadevices or substrates containing VO_2.

There are many methods commonly used to characterize the IMT in VO_2, such as X-ray diffraction (XRD) and Raman spectroscopy, which follow the transition through structural changes, and infrared spectroscopy, which follows the transition through changes in the electronic and optical properties. Another useful technique is differential scanning calorimetry (DSC), which is useful for identifying the transition temperature of VO_2 products, especially when the transition temperature is engineered to be higher or lower than that found in native VO_2 through doping.

X-ray diffraction is a technique that takes advantage of the interaction between generated X-rays and a crystalline substance to identify the unit cell and lattice parameters of the crystal. As mentioned previously, the VO_2 IMT involves a structural transition from the monoclinic to rutile crystal structure, during which, lattice parameters and the unit cell size shift. This change in lattice parameters and unit cell can be detected to give an XRD pattern before and after the structural transition, as was done in a study by Okimura et al. In this study, *in situ* XRD was performed on epitaxial VO_2 films grown on c-Al_2O_3 substrates to observe the crystal structure in VO_2 throughout a thermally-induced IMT. As the sample was gradually heated from 22°C to 104°C, there was a shift in the pattern, especially noticeable in the $(020)_m$ reflection peak around $2\theta = 40°$ corresponding to a lattice spacing of 2.25 Å in the monoclinic M1 phase, which shifted to $2\theta = 39.72°$, or 2.27 Å, upon transition to the rutile R phase.[37]

Another characterization technique that observes the structural changes throughout the IMT is Raman spectroscopy, which relies on the unique lattice vibrations of crystal structures to form a characteristic and almost fingerprint-like spectrum for different compounds. In the

monoclinic structure of VO_2, the V^{4+} ions are arranged in a dimerized pattern, with average distances of 2.6 Å and 3.19 Å between them. However, upon transitioning to the rutile phase, the V^{4+} ions are equally spaced along the *c*-axis and located in an octahedral site, surrounded by six oxygen ions. Due to the increased symmetry in the high temperature rutile phase, all but four of the Raman-active phonons in the monoclinic phase disappear during the transition, as observed by Pan and coworkers.[38]

Although the structural transition can be directly observed throughout the IMT, the electronic transition is often indirectly observed through techniques that measure electronic and optical properties of materials. One such method is infrared spectroscopy, which measures the interaction of infrared light with matter, and is affected by the materials' intrinsic properties. VO_2 is unique, in that it is infrared-transmitting in the insulating state, and infrared-reflecting in the metallic state. Therefore, when VO_2 undergoes its IMT, its ability to reflect infrared wavelengths sharply increases, which is shown in the reflectance spectra.[31]

Many characterization methods focus on measuring aspects of the phase transition and its effect on the material, but in some studies, measuring the actual phase transition temperature is required. In these cases, differential scanning calorimetry is useful, as it measures the heat flow into or out of a sample as it is maintained at the same temperature as a reference. In order for VO_2 to undergo the phase transition, heat input is required and so at the transition temperature, the increased flow of heat is recorded as a peak on DSC curve, plotting heat flow versus temperature.[39] Upon cooling, the DSC curve also records a peak where there is a sudden out-flow of heat from the sample, thus completing the heating and cooling cycle. Through the use of DSC, as well as other characterization methods, such as the ones explained previously, the IMT of VO_2 can be more thoroughly understood.

Methods of VO_2 Synthesis

There are many methods to synthesize VO_2, including a vapor-phase deposition approach, such as chemical vapor deposition (CVD) and DC reactive ion sputtering,[11] as well as solution-based methods, such as solvothermal[40] and colloidal synthesis.[31] There are pros and cons to each method and the VO_2 product formed, and the proper synthesis can be chosen depending on what characteristics the VO_2 particles need to exhibit.

Vapor-phase deposition methods allow for synthesis to occur on a large scale and are commonly used in industry manufacturing for the fabrication of materials, such as semiconductors,[41] and academic research.[42, 43] In these types of syntheses, a bulk material is used as a source to then be deposited in nano- or micro-scale dimensions, whether that be particles or film. These methods often allow products to be relatively consistent and reproducible, normally for a lower cost, but can also have limitations. For example, nanoparticles resulting from vapor-phase deposition methods, such as DC-reactive ion sputtering or CVD,[44] are large and non-uniform, which can limit their utility in applications requiring arrays or films of monodisperse particles. In a VO_2-based metadevice, published in 2016, the active VO_2 layer was synthesized by DC-reactive ion sputtering. This resulted in large, non-uniform particles that made up a >200 nm film. In this particular situation, the large particles detracted from the metadevice response, as inducing the IMT in the entire film of VO_2 was not possible due to a localized response around the current source.[11]

In such situations where polydisperse VO_2 particles are not acceptable and can hamper the insulator-to-metal effect and properties, a solution-based method is desirable, where the size and shape of the particles can be more easily controlled. Two common solution synthesis approaches are solvothermal synthesis or colloidal synthesis.[31] In solvothermal synthesis, VO_2

is formed by reacting vanadium precursors, such as V_2O_5 or $VOSO_4$, in an aqueous solution mixture containing a reducing agent, such as hydrazine, and then allowing the amorphous products to continue crystallization in an autoclave.[40] This, however, results in larger, and sometimes more polydisperse particles. Colloidal synthesis offers the most control of size and particle dispersity when synthesizing VO_2 nanoparticles, however, only one preparation method exists at this point. In colloidal syntheses, a metal precursor is added to a solution that often contains a reducing agent, along with other compounds, such as capping agents and solvents. Specifically, for the colloidal synthesis of VO_2, oleylamine is added in significant excess, and acts as both the reducing and capping agent, preventing aggregation of the VO_x nanoparticles and allowing them to be suspended in nonpolar solutions, such as hexanes.[31] Additionally, the presence of an alcohol is essential to form the vanadium-oxygen bonds, via the reaction between the vanadium chloride and 1-octadecanol.[45]

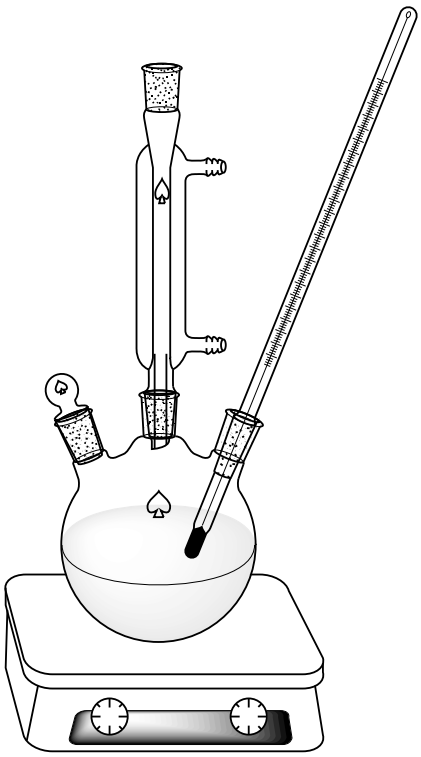

Figure 3. A typical reaction setup for colloidal synthesis, using a round-bottom flask, thermocouple, and condenser attached to a Schlenk line. Illustration drawn by Margeaux Bull.

Silica Coating for Stability

In many cases of colloidal synthesis, the inorganic nanoparticles are relatively stable, but if they are to be used in any industrial, commercial, or large-scale setting, stability and resistance to decomposition must be considered and monitored. In addition, colloidal particles can easily aggregate, which poses a problem when they are in solution or to be used in manufacturing processes of thin films and other materials. A popular method to overcome these issues is silica coating to create a core-shell nanoparticle that results in a stable product with low reactivity that can be further surface-functionalized to allow for novel properties and applications.

Silica coating methods are typically carried out in solution-based systems, and this allows for a significant control over the shell thickness and pore sizes, as well as the conformity and monodispersity of the resultant particles. There are numerous strategies to silica coat nanoparticles, ranging from the classic Stöber method to the reverse microemulsion method. In the classic Stöber method, the nanoparticles are coated through the hydrolysis and condensation of a silicate precursor, catalyzed in an aqueous solution. The silicate precursor, often in the form of sodium silicate or tetraethyl orthosilicate (TEOS), is hydrolyzed and condensed to form a silica layer around the nanoparticle surface. The reactions can be acid- or base-catalyzed, although the base-catalyzed reaction proceeds more quickly due to the acid-catalyzed reaction forming silanol intermediates.[46] In a base-catalyzed reaction, the particles are initially dispersed in a solution of the catalyst, which is often a mixture of ammonia, water, and ethanol. The hydroxyl groups present aid in the condensation of the silica shell, and the concentration directly affects the properties of the resulting silica shell, so it is crucial to have the correct ratio of ethanol:water. For example, at lower ratios (up to 2:1), deposition is not

complete, as some of the silicate will remain in solution, but the deposition will nucleate solely on the nanoparticle surface. At larger ratios, most of the silica will nucleate on the nanoparticle surface, but smaller, free silica particles will be present. In addition, a higher water concentration leads to more polydisperse particles and inhomogeneous surfaces. These differences in silica shell coating are believed to be due to the concentration of hydroxyl radicals, where a higher concentration of hydroxyl radicals facilitates the condensation of the silica shell, resulting in a larger and less homogeneous silica network.[47]

In the Stöber method, two reactions occur to yield the silica shell, the first being the hydrolysis of TEOS into silanol monomers, and the second being the condensation of the silanol monomers into a siloxane network. During the initial hydrolysis in a base-catalyzed synthesis, hydroxyl radicals attack the central silicon atom in the silicate precursor, forming a 5-coordinate complex of 4 -OR groups and 1 -OH group. The 4th -OR group acts as a leaving group, resulting in a 3 -OH and 1 -OH complex. The condensation process occurs when a negatively charged $\equiv SiO^-$ attacks a central Si atom, and kicks off an $-OR^-$ group, which continues to form the silica coating. Ammonia is present in solution to catalyze the reaction by ionizing the water molecules to form an ammonium (NH_4^+) ion and the OH^- ion, speeding the reaction up considerably (Figure 4).

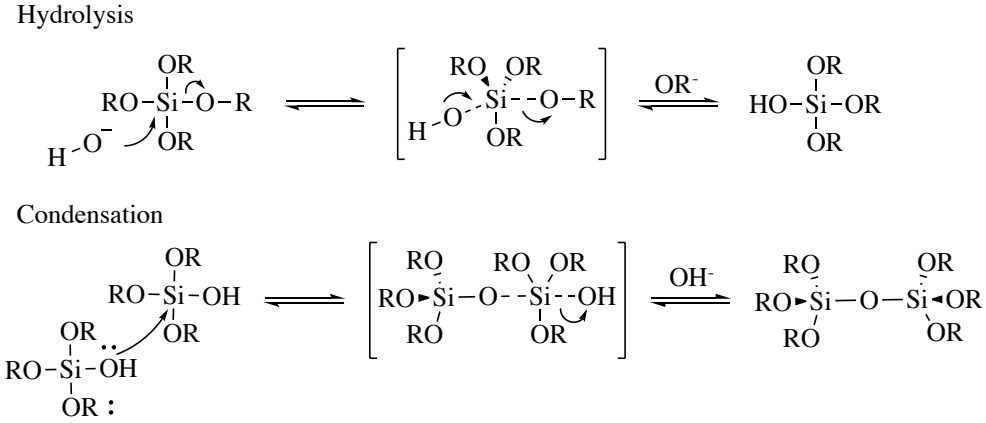

Figure 4. Reaction scheme for the base-catalyzed hydrolysis and condensation of tetraethyl orthosilicate.

In order for a conformal silica coating to form around the particles through the Stöber method, the surface must be conducive to host a silicate ion and the particles themselves must be hydrophilic. To achieve this, the nanoparticle surfaces can be functionalized with a silane coupling agent, commonly used are (3-aminopropyl)trimethoxysilane or (3-aminopropyl)triethoxysilane, through ligand exchange. This allows for a better interaction between the amine functional group and the nanoparticle surface, and to render the surface vitreophilic,[48] while the outward facing silicate group is then hydrolyzed and condensed during the silica coating process.

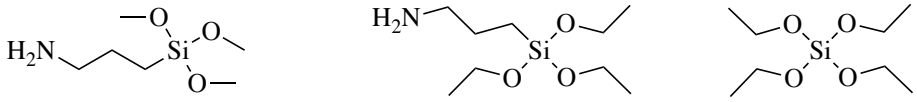

(3-aminopropyl)trimethoxysilane (3-aminopropyl)triethoxysilane tetraethyl orthosilicate

Figure 5. Chemical structures of (3-aminopropyl)trimethoxysilane, (3-aminopropyl)triethoxysilane, and tetraethyl orthosilicate.

In addition to priming or functionalizing nanoparticles that have a low chemical affinity for silica, another silica coating method has been developed, called the reverse-microemulsion method. This process is performed in nonpolar solvents and often uses surfactants that further stabilize the nanoparticles and is often successful for small particles that cannot be coated through a Stöber method. In the common water-in-oil (W/O) reverse-microemulsion approach, micelles are formed, with the aqueous domains stabilized and encapsulated by a surfactant, and homogeneously mixed in an oil or organic solvent. This acts as a "nanoreactor" that allows the aqueous phase to dissolve the polar compounds, and the hydrolysis and condensation of the silicate precursor occurs at the water-oil interface. The reverse-microemulsion approach allows the silica coating of nanoparticles, that are nearly impossible to coat using the Stöber method due to the polydispersity of the silica shell formed on smaller nanoparticles,[49] without a ligand

exchange required. In addition, the reverse-microemulsion method allows for more control to achieve a thinner and monodisperse silica coating.[50]

General Experimental Goals & Strategies

Research concerning VO_2 particles and films has commonly used vapor-phase deposition and solvothermal methods of synthesis, but rarely involve the colloidal synthesis of VO_2. In 2013, Paik and coworkers published a colloidal synthesis method for VO_2 nanoparticles and used dopants to tune the IMT temperature, although the surface chemistry of the particles was not thoroughly explored.[31] The lack of research on the colloidal synthesis of VO_2 nanoparticles has left the behavior and surface chemistry of these particles relatively unknown.

In this work, it was hypothesized that colloidally-synthesized VO_2 would have comparable surface chemistry and would, as a result, behave similarly to other transition metal oxide nanoparticles, including VO_2 synthesized through other methods, such as vapor-phase deposition and solvothermal methods. By exploring the surface chemistry and behavior of these VO_2 nanoparticles, the prospect of surface modification can be realized and allow for further functionalization of these unique particles and use in a wide variety of applications. Recently, an active VO_2-based nanophotonic metadevice was fabricated, although the reconfigurability was current-induced, which resulted in an extremely localized response around the current source and residual Joule heating, leading to a delayed response in the metadevice.[11] Through surface modification of the colloidally-synthesized VO_2 nanoparticles, such limitations can be overcome.

Although this research found that the surface of these colloidally-synthesized VO_2 could not be modified as hypothesized, this research provided further insight into the surface

chemistry and behavior of the nanoparticles. Using this research as a starting point, the possibilities for surface modification and finding the limitations of colloidally-synthesized VO_2 can be further explored, allowing for a better understanding of these particles and further use of VO_2's unique IMT at nanoscale sizes.

CHAPTER 2. MODIFICATION OF COLLOIDALLY-SYNTHESIZED VO_2

Introduction

Colloidally-synthesized amorphous vanadium oxide (VO_x) nanoparticles are less than 10 nm in diameter and relatively monodisperse.[31] These small and monodisperse particles are ideal for building VO_2 layers or thin films in reconfigurable devices and metamaterials, such as a nanophotonic metadevice.[11] However, during the annealing process to oxidize the VO_x to VO_2, the nanoparticles aggregate, resulting in micron-sized VO_2 clusters. In order for these colloidally-synthesized VO_2 nanoparticles to be used successfully in materials and devices, the aggregation and interaction of the particles during the annealing process must be controlled. This research aimed to explore the behavior and surface chemistry of amorphous VO_x and VO_2 nanoparticles through ligand exchange, surface modification, and silica coating, with the goal of preventing the particles from aggregating during the annealing step.

Two common methods of silica coating were used in this research: the Stöber method, which is normally performed in polar solvents, and the reverse microemulsion method, performed in nonpolar solvents. These methods have previously been used to coat many different types of nanoparticles in silica, ranging from noble metal to other transition metal oxide nanoparticles.[48, 51, 52] In order to make the nanoparticle surface more amenable to bonding with the silica groups in the precursors, ligand exchanges or surface modifications can also be performed, often by agitating or sonicating the nanoparticles in solutions of excess ligand.

The native ligand present on amorphous VO_x nanoparticles after colloidal synthesis is oleylamine, a molecule containing an 18-carbon chain, functionalized with an amino group (Figure 6). This allows the polar amino group to bind to the VO_x surface, while using the nonpolar carbon chain to interact with nonpolar molecules, allowing the VO_x nanoparticles to

readily disperse in hexanes. Three compounds were used during the ligand exchange and surface modification attempts prior to silica coating – hexadecyltrimethylammonium bromide (CTAB), (3-aminopropyl)trimethoxysilane (APTMS), and nitrosonium tetrafluoroborate ($NOBF_4$). Hexadecyltrimethylammonium bromide is a common surfactant used in the silica coating of nanoparticles.[53] Similar to oleylamine, it has a hydrocarbon chain, although it contains a cationic head (Figure 6). In typical silica coating procedures, CTAB is the "shape-inducing agent" and forms micelles which surround the nanoparticles during the silica coating process and give an anchor for mesoporous silica formation.[53] In this research, it was hypothesized that the CTAB would form a bilayer with the native oleylamine ligands, with both carbon chains orienting towards each other, and the polar head groups facing inward toward the particle and outward toward the solution. This would theoretically allow the VO_x nanoparticles to be dispersed in polar solvents, such as ethanol and water, which are commonly used for Stöber method silica coating. APTMS was also chosen as a ligand to perform the exchange with, as it is a common silane coupling agent used for silica coating.[54] The amino group on one end is identical to the oleylamine amino group and was hypothesized to bind with similar strength. The opposite end of the compound contains a silicon atom surrounded by three methoxy groups, allowing for the condensation of silicate groups during the silica synthesis (Figure 6).

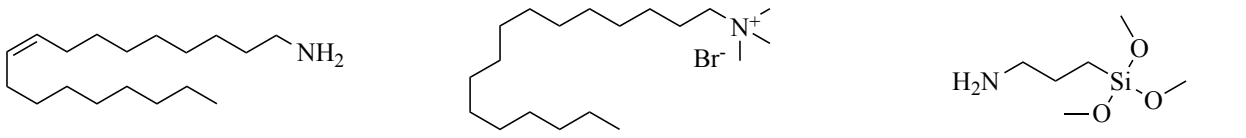

Oleylamine Hexadecyltrimethylammonium bromide (3-aminopropyl)trimethoxysilane

Figure 6. Chemical structures of oleylamine, hexadecyltrimethylammonium bromide, and (3-aminopropyl)trimethoxysilane.

The last ligand identified for exchange was $NOBF_4$, shown to be a useful ligand for making hydrophobic nanoparticles hydrophilic, which can also be readily displaced by other compounds via secondary ligand-exchange.[55]

This research, motivated by the prospect of being used in a metadevice, aimed to modify the surface of the amorphous VO_x nanoparticles prior to oxidation to VO_2, using various ligands and silica coating methods, based upon the hypothesis that these vanadium oxide nanoparticles would behave similarly to other transition metal oxide nanoparticles, as well as VO_2 synthesized through other methods.

Experimental

Materials

Vanadium(V) oxychloride [99%], oleylamine [technical grade, 70%], 1-octadecanol [95%], titanium foil [thickness 0.25 mm, 99.7% trace metals basis], hexadecyltrimethylammonium bromide [>99%], tetraethyl orthosilicate [reagent grade, 98%], (3-aminopropyl)trimethoxysilane [97%], ammonia [28% NH_3 in H_2O], nitrosonium tetrafluoroborate [95%], Igepal CO-520, dichloromethane [reagent grade, ≥99.5%], acetonitrile [reagent grade, ≥99.5%], and cyclohexane [reagent grade, ≥99%], were purchased from Millipore Sigma. Sodium hydroxide, hexanes, toluene, and ethanol, all analytical grade, and glass slides were purchased from VWR. Silicon wafers [50.8 mm, <100> orientation] were purchased from University Wafer. All chemicals were used as received.

Methods

Colloidal Synthesis of Amorphous Vanadium Oxide Particles: Adapting a previously published VO_x procedure,[31] 2 g 1-octadecanol (7.4 mmol) and 7.5 mL oleylamine were added to

a 50 mL 3-neck round-bottom flask with a reflux condenser, thermometer, and rubber septum. The mixture was placed under vacuum and heated at 120°C for 60 min. After placing the flask under argon, a needle was placed in the rubber septum to allow argon flow. In the glovebox, 100 uL vanadium(V) oxychloride (1.1 mmol) was added to approximately 500 uL dry hexanes, then removed in a vial and completely injected into the flask. The solution was then heated to 215°C and allowed to react for 20 min, after which, the heating mantle was removed, and the reaction was allowed to cool to room temperature. The particles were then cleaned initially with toluene and ethanol via centrifugation, and this was repeated a second time using hexanes and ethanol. The resulting nanoparticles were dispersed in hexanes for further use.

Annealing of VO_x Nanoparticles to Obtain VO_2 Nanoparticles: The VO_x nanoparticles in hexanes were dropcast onto titanium foil and placed in a Thermo Scientific™ Lindberg/Blue M tube furnace under argon. The program was then set to the following standard parameters: held at room temperature for 30 min, heated to 475°C in 45 minutes, remaining at this temperature for 4 hours, and then cooled to room temperature. The resulting product was then scraped off to characterize with TEM and XRD or analyzed by XRD directly on the titanium foil. The effect of using various substrates on the resulting VO_2 crystallinity was also studied. Substrates used included glass slides and silicon wafers.

Attempted Silica Coating of VO_x Nanoparticles via CTAB Modification: Approximately 1 mL VO_x nanoparticles in hexanes (10 mg/mL) were added to a 20 mL septum-capped vial and vacuum was pulled on the vial to evaporate the hexanes. 10 mL 0.8 mM $CTAB_{(aq)}$ solution was then added, and the solution was probe sonicated in the vial over an ice bath, using a Misonix Sonicator 400, on ice at 30% amplitude and set to sonicate for 5 sec at a

time, with a 3 sec pause in-between, for 3 hours. Variables of the preparation method were studied to observe the effect on the dispersibility of the particles in the aqueous CTAB solutions. The concentration of the CTAB solutions ranged from 0.8 mM to a saturated solution, and the CTAB was also made in a hexanes and an ethanol solution. Additionally, the method of sonication was varied by using a bath sonicator, rather than a probe sonicator.

Using a Mettler Toledo SevenExcellence Multiparameter pH meter, the pH of the solution was adjusted to ~10 by adding 10 mM $NaOH_{(aq)}$ drop-wise. 50 uL 20% TEOS in ethanol solution was then added and the sample was allowed to stir overnight. The resulting particles were then cleaned via centrifugation, using hexanes and ethanol. The particles were then dispersed in hexanes to observe via TEM. To see if the sequence of adding the VO_x nanoparticles affected the resulting particles, the pH of the solution was adjusted prior to adding the VO_x nanoparticles.

Attempted Silica Coating of VO_x Nanoparticles via APTMS Exchange: In a 20 mL vial, 100 uL VO_x nanoparticles in hexanes (13 mg/mL) were centrifuged and redispersed in 5 mL of a 9% APTMS in ethanol solution. The vial was then set in a bath sonicator while 50 uL TEOS was added and the solution was allowed to sonicate for 5 min, after which, 20 uL ammonia was added. The solution was then sonicated for 4 hours and the resulting particles were washed twice via centrifugation, using hexanes and ethanol. The particles were then dispersed in hexanes to observe via TEM. To see if varying components of the synthesis would result in APTMS-functionalized VO_x nanoparticles, the amount of APTMS added, solvent, and temperature were also varied.

Attempted Silica Coating of VO_x Nanoparticles via $NOBF_4$ Exchange: Adapting a previously published procedure, two methods of $NOBF_4$ exchange were attempted.[55] In accordance with the first method, 7 mg $NOBF_4$ was dissolved in 5 mL dichloromethane in a 20 mL vial. 5 mL VO_x nanoparticles in hexanes (5 mg/mL) were then added and the solution was stirred for 15 minutes. Per the second method, 5 mL acetonitrile was added to 5 mL VO_x nanoparticles in hexanes (5 mg/mL), after which, 5 mg $NOBF_4$ was added. The solution was stirred for 10 minutes.

Attempted Silica Coating of VO_x Nanoparticles Using Silica Prep for Metal Oxides: Adapting a previously published procedure,[56] in a 40 mL vial, 2 mL Igepal CO-520 were dissolved in 35 mL cyclohexane and degassed with argon for 15 min. 1 mL VO_x nanoparticles in cyclohexane (9 mg/mL) was added and the solution was degassed for another 15 min. The vial was then stirred on a hot plate while 200 uL ammonia was added drop-wise. The solution was allowed to stir for 5 min, after which, 110 uL TEOS was added to the vial and the solution was stirred overnight under an argon blanket. The particles were washed twice via centrifugation using acetone and hexanes and stored in acetone.

Characterization

Powder X-ray diffraction (XRD) data were collected using a PANalytical Empyrean X-ray diffractometer using Cu K-α radiation. Transmission electron microscopy (TEM) images were collected from a JEOL 1200 EX II microscope operating at 80 kV. Average nanoparticle diameter was obtained using ImageJ and contained 200 particles for the sample.

Results and Discussion

The standard VO_x nanoparticle synthesis was derived from a publication from Paik and coworkers.[31] In the original synthesis, the vanadium oxychloride was added to the solution under ambient air conditions, but since vanadium oxychloride is reactive in air and readily hydrolyzes, we performed the reaction under inert conditions. The initial iterations of the modified VO_x nanoparticle syntheses were performed under argon blanket, which resulted in a thick, brown, sludge-like product. This product contained the amorphous VO_x nanoparticles, but also likely contained residual organic compounds derived from the oleylamine and 1-octadecanol. To attempt to prevent this, argon flow was achieved by inserting a needle into the round bottom flask via the rubber septum, allowing the solution to vent while reacting. Through the use of argon flow, rather than an argon blanket, the VO_x nanoparticles were able to be cleanly precipitated out of solution onto the sides of the centrifuge tube, leaving a clear, brown supernatant. VO_x nanoparticles from the subsequent colloidal reactions were amorphous, as shown by the XRD pattern (Figure 7). Although not crystalline, these VO_x nanoparticles were relatively monodisperse with an average diameter of 4.9 ± 0.6 nm, when examined by TEM (Figure 8).

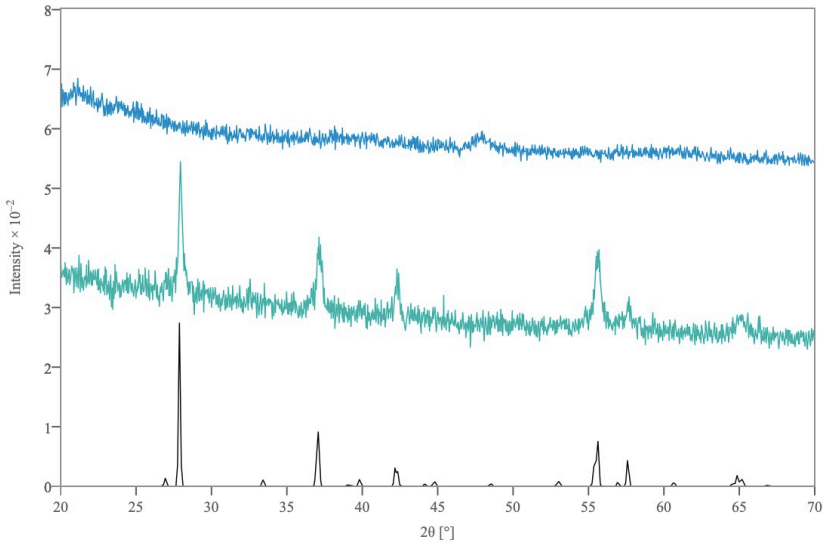

Figure 7. XRD patterns of products throughout the synthesis of VO_2 nanoparticles. The top pattern (blue) is the VOx nanoparticles after the colloidal synthesis. The middle pattern (green) is the VO_2 nanoparticles after the annealing process. The bottom pattern (black) is the simulated VO_2 (M) pattern, ICDD PDF# 97-002-4926.

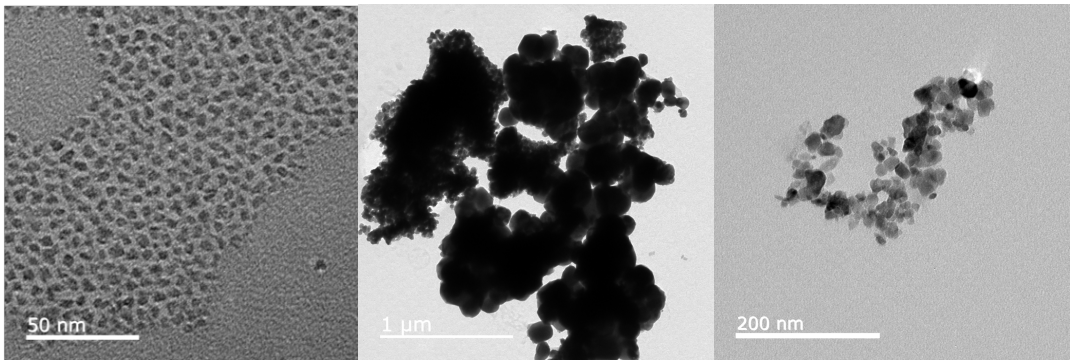

Figure 8. TEM images of VO_x nanoparticles after colloidal synthesis (left), VO_2 nanoparticles after the annealing process, but prior to probe sonication (center), VO_2 nanoparticles after the annealing process and probe sonication (right).

In order to acquire VO_2 nanoparticles, the amorphous VO_x nanoparticles must be oxidized through an annealing process, as there are many vanadium oxide polymorphs and vanadium oxidation states present at room temperature.[57] Previous annealing procedures to achieve VO_2 have used precise atmospheres containing exact ratios of oxygen and inert gas. However, the methods to achieve precise atmospheres were not accessible, and so annealing procedures in this research were performed under argon. Using the standard annealing procedure, the XRD pattern of the resulting VO_2 nanoparticles annealed on titanium foil matched the simulated VO_2 (M) pattern (Figure 7). As observed by TEM, the nanoparticles

appeared to aggregate during the annealing process (Figure 8). This resulted in large, micron-sized aggregates of crystalline VO_2. This aggregation made it difficult to image the individual VO_2 nanoparticles, so they were briefly probe sonicated prior to imaging on the TEM a second time. The resulting particles after probe sonication were clearly defined with relatively smooth edges, suggesting that the process during annealing was aggregation, rather than sintering together (Figure 8).

To see whether the substrate the VO_x was annealed on would affect the crystallinity of the VO_2 product, two substrates were compared against the titanium foil – a glass slide, and a silicon wafer. Using the standard annealing conditions successful in annealing the VO_x on titanium foil previously, the VO_x nanoparticles were dropcast on these substrates and then annealed under argon at 475°C for 4 hours in the tube furnace. The crystallinity of the product can be inferred from the XRD pattern, as the sharper and more intense the peaks, the more crystalline the sample. The annealing conditions for all of these samples were identical, and by looking at the XRD patterns, specifically the [011] and [211] reflections around $2\theta = 27°$ and 55°, it is apparent that the titanium foil resulted in the most crystalline VO_2 product, whereas the silicon wafer resulted in the least crystalline VO_2 product (Figure 9).

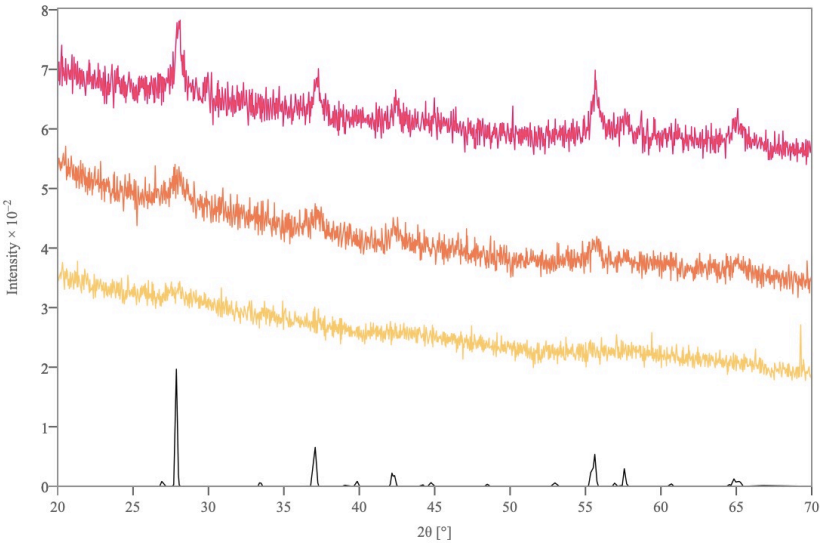

Figure 9. XRD patterns of VO_x annealed on various substrates. The top pattern (red) is the VO_x sample annealed on titanium foil. The upper middle pattern (orange) is the VO_x sample annealed on the glass slide. The lower middle pattern (yellow) is the VO_x sample annealed on the silicon wafer. The bottom pattern (black) is the simulated VO_2 (M) pattern, ICDD PDF# 97-002-4926.

This result is likely due to the amount of oxygen atoms present at the surface of the substrates, which can allow for diffusion of the oxygen atoms to the oxygen deficient VO_x nanoparticles. These oxygen atoms also facilitate crystallization of the VO_x nanoparticles by allowing rearrangement of the vanadium and oxygen atoms on the surface. Titanium is known to have a native oxide layer around 8 nm,[58] whereas the silicon native oxide layer is less, around 5.5 nm.[59] Additionally, the bond dissociation energy of the O-Ti bond is lower than the O-Si bond, at 660 kJ/mol, compared to 800 kJ/mol.[60] Titanium has a thicker oxide layer, with the bonds between O and Ti being easier to break due the bond dissociation energy, and this likely results in more facilitated movement of the surface atoms and atoms in the VO_x nanoparticles. The glass slide is amorphous silicon dioxide, SiO_2, although the O-Si bond is stronger, making it more difficult for the surface oxygen atoms to diffuse and aid in VO_x crystallization. The resulting crystallinity after using a silicon wafer also corresponds to this reasoning, as silicon

has the thinner oxide layer and relatively strong O-Si bonds, which would lead to restricted movement of the substrate surface groups.

Moving forward after identifying the proper synthesis methods to achieve the VO_x, and subsequent VO_2 nanoparticles, the surface chemistry of the VO_x and VO_2 particles was studied as multiple strategies were employed to modify the surface of the nanoparticles. This was done in preparation for fabricating the VO_2 layer within the metadevice. While two silica coating methods, the Stöber method and reverse microemulsion method, were attempted, ligand exchanges and modifications were also performed on the VO_x nanoparticles prior to the Stöber process. This was done to facilitate the interaction between the VO_x nanoparticles and the silane groups forming the silica coating.

The CTAB modification of the VO_x nanoparticles was considered generally unsuccessful. Variables studied were the concentration of the CTAB solution, the solvent used for the CTAB solution, method of introducing the CTAB solution to the VO_x nanoparticles, and method of agitation. Solutions of CTAB, with concentrations of 0.8 mM, 10 mM, 50 mM, and an excess of CTAB, were prepared in hexanes, ethanol, and water. By changing the solvent, it was hypothesized that the more polar solutions would destabilize the hydrophobic VO_x particles and encourage the CTAB to form a bilayer with the oleylamine ligands to allow the polar head groups of CTAB to face outward into solution and stabilize the particles. The concentration of CTAB as also changed in order to increase the amount of CTAB present in solution and available to form a bilayer with the oleylamine ligands. The VO_x nanoparticles were then added to these solutions while dispersed in hexanes, and the resulting mixtures were sonicated using a probe sonicator. Additionally, a bath sonicator was used to sonicate the solutions constantly, for a longer amount of time with a lower energy which also resulted in a gradual temperature

increase to around 60°C, as opposed to the probe sonicator, which sonicated the solution for short bursts of time with a higher energy. The consistent result after carrying out each method was VO_x nanoparticle aggregation in solution, resulting in the particles crashing out of the solution. It was hypothesized that introducing CTAB to the VO_x nanoparticles would result in a bilayer being formed from the carbon chains of CTAB and oleylamine orienting toward each other, leaving the polar heads facing inward toward the particle and outward toward the polar solution. Prior to introducing the CTAB to VO_x, it was dispersed in ethanol and water, both of which are polar solvents, which would result in cylindrical micelles being formed, due to the amphiphilic nature of CTAB.[61] The solutions were sonicated to disrupt the micelles and encourage the CTAB to form a bilayer around the VO_x nanoparticles. However, due to limited or no van der Waals interaction between the hydrocarbon chains of CTAB and oleylamine, bilayers did not form, allowing the VO_x nanoparticles to aggregate and crash out of solution. It is possible that agitation of the solution was not the proper method to disrupt the micelles and form a bilayer around the VO_x nanoparticles. Although the probe sonication was done in pulses, the bath sonicator was run continuously and allowed to heat up to around 60°C. Recent research has shown that a bilayer of lauric acid, which is structurally similar to oleylamine, and CTAB was successfully formed around $CoFe_2O_4$ nanoparticles by heating the lauric-acid capped nanoparticles in an aqueous CTAB solution at 75°C.[62] Given this information, it is possible that increasing the temperature during agitation may successfully initiate bilayer formation.

Additionally, a typical base-catalyzed Stöber synthesis requires the solution to be adjusted to a basic pH so that the proper concentration of hydroxyl groups is present. Using one of the CTAB solutions that appeared to have a very small amount of VO_x nanoparticles left

dispersed, due to the grey coloring of the solution, the pH adjustment and silica coating were attempted, albeit unsuccessfully. While raising the pH from the original pH of around 4, by adding 10 mM $NaOH_{(aq)}$ dropwise, the VO_x nanoparticles completely crashed out of solution and stuck to the walls of the glass vial around pH 7-8. Based on the difficulty to form an oleylamine/CTAB bilayer around the VO_x nanoparticles while in polar solvents, the oleylamine-capped VO_x nanoparticles likely had little or no CTAB present to stabilize them in the aqueous solution. As the hydrocarbon chain on oleylamine is hydrophobic, the particles were already unstable in solution. Due to the presence of additional hydroxyl ions throughout the pH adjustment, the VO_x nanoparticles in solution were further disrupted and it was likely more favorable for the particles to aggregate and orient the hydrocarbon chains in a cluster, rather than being individually surrounded by hydroxyl ions.[61] After adding the TEOS in ethanol, TEM indicated that only silica particles were present, confirming that no VO_x nanoparticles were coated in silica.

During attempts to exchange the oleylamine ligands for APTMS, the amount of APTMS present in solution, solvent used, and temperature of solution were varied. In order to increase the concentration of APTMS in solution and encourage exchange with oleylamine, the volumes of APTMS added were changed. The experiments used 20 uL, 100 uL, 150 uL and 200 uL APTMS. Additionally, the VO_x nanoparticles were sonicated in solutions of APTMS dissolved in various solvents, including toluene, water, and ethanol, to examine if varying the solution polarity would facilitate ligand exchange by stabilizing the exposed silane groups. For all of the exchange attempts, the VO_x nanoparticles were dispersed in solution during sonication. However, upon removing the particles from the bath sonicator, they consistently aggregated and crashed out of solution, similar to the results seen during the CTAB modifications. In addition

to increasing the concentration of APTMS in solution, and the solvent used, the VO_x nanoparticles were stirred at 50°C, rather than sonicated at room temperature, to encourage ligand exchange. This strategy was not successful either, and also resulted in the particles aggregating and crashing out of solution after being removed from stirring. APTMS has an amino group identical to oleylamine, leading one to believe they would readily exchange for each other as the interactions with VO_x nanoparticles would be very similar. However, APTMS has a large and bulky silane group present at the opposite end, which could be too sterically hindered to access the VO_x nanoparticle surface at reasonable concentrations, compared to oleylamine, leading to a higher ratio of oleylamine to APTMS ligands present on the nanoparticles. This would lead to the inability of VO_x to be dispersed in polar solvents, which was observed as particles aggregated and crashed out of solution.

Due to the difficulty in exchanging the ligands through sonication, a different approach using $NOBF_4$ was taken. The process involved dispersing the VO_x nanoparticles in solutions of $NOBF_4$ in dichloromethane and acetonitrile.[55] After 10 minutes, the color of the solutions turned green and a yellowish-brown color, indicating a possible decomposition into V^{3+} and V^{5+} ions. The BF_4^- ion is strongly nucleophilic, so it is possible that the anion was able to attack surface vanadium ions, decomposing the nanoparticles. Additionally, the VO_x nanoparticles were amorphous, resulting in a disordered network and distorted structure and weaker atomic bonding.

In addition to syntheses using the Stöber method, the reverse microemulsion method was also used. As these methods have been used to coat metal oxide nanoparticles in silica,[56] it was inferred that it would be successful to coat the vanadium oxide nanoparticles as well. To first confirm that the reverse microemulsion method would be successful in coating metal oxide

nanoparticles, the procedure to coat manganese oxide, MnO, nanoparticles in silica by Schladt et al. was reproduced.[63] After using the reverse microemulsion method to silica coat the manganese oxide nanoparticles, a thin layer of silica surrounding the particles was identified by the difference in contrast apparent in the TEM image (Figure 10). These results indicated that the reverse microemulsion method was able to successfully coat one type of metal oxide nanoparticles and would possibly coat vanadium oxide nanoparticles as well.

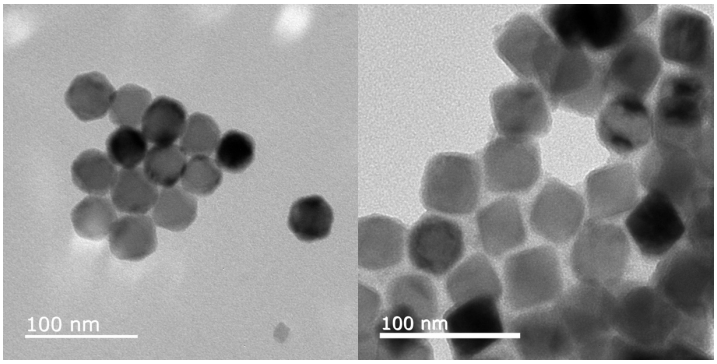

Figure 10. TEM image of the manganese oxide particles before (left) and after (right) silica coating, using the reverse microemulsion method, reproduced from the synthesis outlined by Schladt et al.[63]

In attempts to coat the VO_x nanoparticles using the reverse microemulsion method, the amount of ammonia and TEOS added to the solutions were varied, as well as the order these compounds were added in. Throughout the experiments, 50 uL, 100 uL, 150 uL, and 200 uL of ammonia were added. Increasing the amount of ammonia added would effectively increase the concentration of hydroxyl radicals, facilitating and speeding the hydrolysis of TEOS to encourage the formation of silica. Additionally, the amount of TEOS added was varied, including 20 uL, 30 uL, 50 uL, and 100 uL, to increase the concentration of silica in solution. In order to examine if the order the ammonia and TEOS were added would affect the resulting emulsion and micelle formation, the TEOS was also added before the ammonia. However, all experiments using the reverse microemulsion method resulted in only silica particle formation, which was identified using TEM (Figure 11). The contrast of particles in a TEM image is

directly proportional to the molecular weight of the compound, and the light contrast of these particles corresponds to silica, rather than any of the much heavier vanadium oxide species, which would appear much darker in contrast.

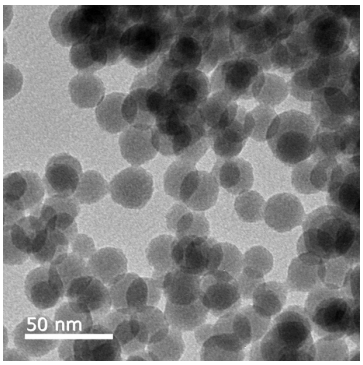

Figure 11. TEM image of a typical silica coating synthesis product containing only silica particles. This image was taken from a reverse microemulsion method product.

The formation of only silica spheres indicated that there was a difference between the surface chemistry of the manganese oxide and vanadium oxide nanoparticles, possibly due to a difference in zeta potential. Zeta potential is a measurement based on how a particle's surface charge interacts with its surrounding conditions. The zeta potential in nanoparticles is easily affected, as they have a higher mean bond energy per atom, due to their high surface area to volume ratio. This can lead to the leaching of ions and atoms from the surface, resulting in surface vacancies that increase the surface charge.[64] Silica is known to have a negative zeta potential,[65] whereas various manganese oxide phases, including MnO, have been shown to have a positive zeta potential under pH 10,[66, 67] resulting in a favorable interaction that facilitates silica coating of these nanoparticles. It has also been shown that TiO_2 with a positive zeta potential were successfully coated in silica, while the same silica coating reaction was unsuccessful using TiO_2 with a negative zeta potential.[68] Using this knowledge, a possible explanation for the formation of silica spheres, rather than silica-coated VO_x, is that the VO_x

nanoparticles have a negative zeta potential in the reverse microemulsion method conditions, due to vanadium atom deficiencies on the surface, preventing a silica shell from forming.

Additionally, as the reactions progressed, the color of the solution consistently changed from dark brown or almost black to light brown or nearly colorless. This was a visual indication that the VO_x nanoparticles were decomposing during the process, although the solution colors were not able to be correlated with the known colors of vanadium ions and oxidation states.[69] The catalyst most commonly used in reverse microemulsion methods is ammonia, and using the reasoning presented for $NOBF_4$, the nucleophilic ammonia likely attacked the surface vanadium ions in a similar fashion, resulting in the VO_x nanoparticles decomposing.

The silica coating procedures in the Stöber method and reverse microemulsion method are generally straightforward, and during this research, it was found that varying the amount of reactants added during the reaction only affected the resulting silica properties, such as thickness and porosity, rather than whether or not the silica shell formed around the VO_x nanoparticles. Overall, these experiments indicated that there was a significant difference in the behavior and surface chemistry of the colloidally-synthesized vanadium oxide nanoparticles and other transition metal oxide nanoparticles, proven by the unsuccessful experiments attempting to exchange the oleylamine ligands and modify the VO_x nanoparticle surface using methods previously successful for other nanoparticles. Due to the minimal research performed on colloidally-synthesized VO_2, this study of the surface chemistry of VO_x and VO_2 contributed useful knowledge on the behavior of colloidal VO_x during methods and syntheses commonly used with other metal oxide nanoparticles and solvothermally-synthesized VO_2.

Future Directions

In summary, it was determined that the colloidally-synthesized vanadium oxide exhibits much different behavior, and evidently has different surface chemistry, than other transition metal oxide nanoparticles. Initial research attempts using methods previously successful with other metal oxide nanoparticles, including VO_2, to silica coat the nanoparticles and perform ligand exchanges proved to be unsuccessful. Although the vanadium oxide nanoparticles were unable to be coated in silica, the silica coating process, whether using the Stöber or reverse microemulsion method, is normally successful in leaving a silica shell around the particle and modifying the volumes of reagents added will only result in different properties, such as thickness and porosity, of the silica shell. Due to the complete absence of vanadium oxide nanoparticles in solution after silica coating syntheses, the instability of these nanoparticles during the typical silica coating processes is apparent.

Future research in this area of colloidally-synthesized VO_2 could be expanded to include other studies on the behavior of VO_2 to lead to fundamental understanding of the nanoparticles. VO_2 has many practical applications, ranging from industry and medicine, to the military, but the use of VO_2 in nanomaterials is currently limited by the lack of fundamental knowledge of the colloidal nanoparticles. As found in this research, the colloidally-synthesized VO_2 did not interact with the ligands or nucleophilic reagents during the silica coating process as other transition metal oxides have, so studying coupling agents with other functional groups that have a higher affinity for the vanadium particles and other non-nucleophilic catalysts would yield better understanding of the nanoparticle's behavior and allow for further surface modification. Additionally, the VO_x nanoparticles must be annealed to VO_2 in a tube furnace, resulting in an aggregation of the particles. In order to allow more versatility of the product, solution-based

annealing of the VO_x nanoparticles without aggregation in solution would be advantageous, as the resulting VO_2 could be used for further colloidal synthesis modifications or hybrid nanoparticle synthesis, or easily deposited as mono- or multi-layer films.

References

1. Pendry, J. B., Negative Refraction Makes a Perfect Lens. *Phys. Rev. Lett.* **2000,** *85* (18), 3966-3969.

2. Zigoneanu, L.; Popa, B.-I.; Cummer, S. A., Three-dimensional broadband omnidirectional acoustic ground cloak. *Nat. Mater.* **2014,** *13*, 352.

3. Schurig, D.; Mock, J. J.; Justice, B. J.; Cummer, S. A.; Pendry, J. B.; Starr, A. F.; Smith, D. R., Metamaterial Electromagnetic Cloak at Microwave Frequencies. *Science* **2006,** *314* (5801), 977.

4. Liu, R.; Ji, C.; Zhao, Z.; Zhou, T., Metamaterials: Reshape and Rethink. *Engineering* **2015,** *1* (2), 179-184.

5. Fang, N.; Lee, H.; Sun, C.; Zhang, X., Sub-Diffraction-Limited Optical Imaging with a Silver Superlens. *Science* **2005,** *308* (5721), 534.

6. Liu, N.; Mesch, M.; Weiss, T.; Hentschel, M.; Giessen, H., Infrared Perfect Absorber and Its Application As Plasmonic Sensor. *Nano Lett.* **2010,** *10* (7), 2342-2348.

7. Goldflam, M. D.; Driscoll, T.; Chapler, B.; Khatib, O.; Marie Jokerst, N.; Palit, S.; Smith, D. R.; Kim, B.-J.; Seo, G.; Kim, H.-T.; Ventra, M. D.; Basov, D. N., Reconfigurable gradient index using VO_2 memory metamaterials. *Appl. Phys. Lett.* **2011,** *99* (4), 044103.

8. Dicken, M. J.; Aydin, K.; Pryce, I. M.; Sweatlock, L. A.; Boyd, E. M.; Walavalkar, S.; Ma, J.; Atwater, H. A., Frequency tunable near-infrared metamaterials based on VO_2 phase transition. *Opt. Express* **2009,** *17* (20), 18330-18339.

9. Shelton, D. J.; Coffey, K. R.; Boreman, G. D., Experimental demonstration of tunable phase in a thermochromic infrared-reflectarray metamaterial. *Opt. Express* **2010,** *18* (2), 1330-1335.

10. Seo, M.; Kyoung, J.; Park, H.; Koo, S.; Kim, H.-S.; Bernien, H.; Kim, B. J.; Choe, J. H.; Ahn, Y. H.; Kim, H.-T.; Park, N.; Park, Q. H.; Ahn, K.; Kim, D.-S., Active Terahertz Nanoantennas Based on VO_2 Phase Transition. *Nano Lett.* **2010,** *10* (6), 2064-2068.

11. Liu, L.; Kang, L.; Mayer, T. S.; Werner, D. H., Hybrid metamaterials for electrically triggered multifunctional control. *Nat. Commun.* **2016,** *7*, 13236.

12. Morin, F. J., Oxides Which Show a Metal-to-Insulator Transition at the Neel Temperature. *Phys. Rev. Lett.* **1959,** *3* (1), 34-36.

13. Qazilbash, M. M.; Brehm, M.; Chae, B.-G.; Ho, P. C.; Andreev, G. O.; Kim, B.-J.; Yun, S. J.; Balatsky, A. V.; Maple, M. B.; Keilmann, F.; Kim, H.-T.; Basov, D. N., Mott Transition in VO_2 Revealed by Infrared Spectroscopy and Nano-Imaging. *Science* **2007,** *318* (5857), 1750.

14. Yamauchi, T.; Isobe, M.; Ueda, Y., Charge order and superconductivity in vanadium oxides. *Solid State Sci.* **2005,** *7* (7), 874-881.

15. Tselev, A.; Luk'yanchuk, I. A.; Ivanov, I. N.; Budai, J. D.; Tischler, J. Z.; Strelcov, E.; Kolmakov, A.; Kalinin, S. V., Symmetry Relationship and Strain-Induced Transitions between Insulating M1 and M2 and Metallic R phases of Vanadium Dioxide. *Nano Lett.* **2010,** *10* (11), 4409-4416.

16. Cao, J.; Ertekin, E.; Srinivasan, V.; Fan, W.; Huang, S.; Zheng, H.; Yim, J. W. L.; Khanal, D. R.; Ogletree, D. F.; Grossman, J. C.; Wu, J., Strain engineering and one-dimensional organization of metal–insulator domains in single-crystal vanadium dioxide beams. *Nat. Nanotechnol.* **2009,** *4*, 732.

17. Ruzmetov, D.; Gopalakrishnan, G.; Ko, C.; Narayanamurti, V.; Ramanathan, S., Three-terminal field effect devices utilizing thin film vanadium oxide as the channel layer. *J. Appl. Phys* **2010,** *107* (11), 114516.

18. Nakano, M.; Shibuya, K.; Okuyama, D.; Hatano, T.; Ono, S.; Kawasaki, M.; Iwasa, Y.; Tokura, Y., Collective bulk carrier delocalization driven by electrostatic surface charge accumulation. *Nature* **2012,** *487*, 459.

19. Jeong, J.; Aetukuri, N.; Graf, T.; Schladt, T. D.; Samant, M. G.; Parkin, S. S. P., Suppression of Metal-Insulator Transition in VO_2 by Electric Field–Induced Oxygen Vacancy Formation. *Science* **2013,** *339* (6126), 1402.

20. Yin, J.; Matsuda, J.-I.; Shigeaki, N., Three-dimensional reconstruction of magnetic stray fields using reflection electron beam tomography. *J. Phys. D* **1996,** *29* (5), 1116.

21. Granqvist, C. G., Solar Energy Materials. *Adv. Mater.* **2003,** *15* (21), 1789-1803.

22. Granqvist, C. G., Transparent conductors as solar energy materials: A panoramic review. *Sol. Energy Mater. Sol. Cells* **2007,** *91* (17), 1529-1598.

23. Gea, L. A.; Boatner, L. A., Optical switching of coherent VO_2 precipitates formed in sapphire by ion implantation and annealing. *Appl. Phys. Lett.* **1996,** *68* (22), 3081-3083.

24. Driscoll, T.; Kim, H.-T.; Chae, B.-G.; Kim, B.-J.; Lee, Y.-W.; Jokerst, N. M.; Palit, S.; Smith, D. R.; Di Ventra, M.; Basov, D. N., Memory Metamaterials. *Science* **2009,** *325* (5947), 1518.

25. Lee, M. J.; Park, Y.; Suh, D. S.; Lee, E. H.; Seo, S.; Kim, D. C.; Jung, R.; Kang, B. S.; Ahn, S. E.; Lee, C. B.; Seo, D. H.; Cha, Y. K.; Yoo, I. K.; Kim, J. S.; Park, B. H., Two Series Oxide Resistors Applicable to High Speed and High Density Nonvolatile Memory. *Adv. Mater.* **2007,** *19* (22), 3919-3923.

26. Coy, H.; Cabrera, R.; Sepúlveda, N.; Fernández, F. E., Optoelectronic and all-optical multiple memory states in vanadium dioxide. *J. Appl. Phys* **2010,** *108* (11), 113115.

27. Stefanovich, G.; Pergament, A.; Stefanovich, D., Electrical switching and Mott transition in VO_2. *J. Phys. Condens. Matter* **2000,** *12* (41), 8837.

28. Yang, Z.; Ko, C.; Ramanathan, S., Oxide Electronics Utilizing Ultrafast Metal-Insulator Transitions. *Annu. Rev. Mater. Res.* **2011,** *41* (1), 337-367.

29. Goodenough, J. B., The two components of the crystallographic transition in VO_2. *J. Solid State Chem.* **1971,** *3* (4), 490-500.

30. Budai, J. D.; Hong, J.; Manley, M. E.; Specht, E. D.; Li, C. W.; Tischler, J. Z.; Abernathy, D. L.; Said, A. H.; Leu, B. M.; Boatner, L. A.; McQueeney, R. J.; Delaire, O., Metallization of vanadium dioxide driven by large phonon entropy. *Nature* **2014,** *515* (7528), 535-539.

31. Paik, T.; Hong, S.-H.; Gaulding, E. A.; Caglayan, H.; Gordon, T. R.; Engheta, N.; Kagan, C. R.; Murray, C. B., Solution-Processed Phase-Change VO_2 Metamaterials from Colloidal Vanadium Oxide (VO_x) Nanocrystals. *ACS Nano* **2014,** *8* (1), 797-806.

32. Brückner, W., Structural relations between the VO_2 phases. *Cryst. Res. Technol.* **1981,** *16* (3).

33. Whittaker, L.; Patridge, C. J.; Banerjee, S., Microscopic and Nanoscale Perspective of the Metal−Insulator Phase Transitions of VO_2: Some New Twists to an Old Tale. *J. Phys. Chem. Lett.* **2011,** *2* (7), 745-758.

34. Ruzmetov, D.; Senanayake, S. D.; Ramanathan, S., X-ray absorption spectroscopy of vanadium dioxide thin films across the phase-transition boundary. *Phys. Rev. B* **2007,** *75* (19), 195102.

35. Fan, L. L.; Chen, S.; Luo, Z. L.; Liu, Q. H.; Wu, Y. F.; Song, L.; Ji, D. X.; Wang, P.; Chu, W. S.; Gao, C.; Zou, C. W.; Wu, Z. Y., Strain Dynamics of Ultrathin VO_2 Film Grown on TiO_2 (001) and the Associated Phase Transition Modulation. *Nano Lett.* **2014,** *14* (7), 4036-4043.

36. Cavalleri, A.; Tóth, C.; Siders, C. W.; Squier, J. A.; Ráksi, F.; Forget, P.; Kieffer, J. C., Femtosecond Structural Dynamics in VO_2 during an Ultrafast Solid-Solid Phase Transition. *Phys. Rev. Lett.* **2001,** *87* (23), 237401.

37. Okimura, K.; Sakai, J.; Ramanathan, S., In situ x-ray diffraction studies on epitaxial VO_2 films grown on c-Al_2O_3 during thermally induced insulator-metal transition. *J. Appl. Phys.* **2010,** *107* (6), 063503.

38. Pan, M.; Liu, J.; Zhong, H.; Wang, S.; Li, Z.-F.; Chen, X.; Lu, W., Raman study of the phase transition in VO_2 thin films. *J. Cryst. Growth.* **2004,** *268* (1), 178-183.

39. Whittaker, L.; Jaye, C.; Fu, Z.; Fischer, D. A.; Banerjee, S., Depressed Phase Transition in Solution-Grown VO_2 Nanostructures. *J. Am. Chem. Soc.* **2009,** *131* (25), 8884-8894.

40. Son, J.-H.; Wei, J.; Cobden, D.; Cao, G.; Xia, Y., Hydrothermal Synthesis of Monoclinic VO_2 Micro- and Nanocrystals in One Step and Their Use in Fabricating Inverse Opals. *Chem. Mater.* **2010,** *22* (10), 3043-3050.

41. Grudowski, P. A.; Chen, J.; Yeap, C.-F., Semiconductor fabrication process using transistor spacers of differing widths. U.S. Patent 6,864,135 B2, 2005.

42. Park, W. I.; Yi, G. C.; Kim, M.; Pennycook, S. J., ZnO Nanoneedles Grown Vertically on Si Substrates by Non-Catalytic Vapor-Phase Epitaxy. *Adv. Mater.* **2002,** *14* (24), 1841-1843.

43. Zhan, Y.; Liu, Z.; Najmaei, S.; Ajayan, P. M.; Lou, J., Large-Area Vapor-Phase Growth and Characterization of MoS_2 Atomic Layers on a SiO_2 Substrate. *Small* **2012,** *8* (7), 966-971.

44. Podrezova, L. V.; Porro, S.; Cauda, V.; Fontana, M.; Cicero, G., Comparison between ZnO nanowires grown by chemical vapor deposition and hydrothermal synthesis. *Appl. Phys. A* **2013,** *113* (3), 623-632.

45. Niederberger, M., Nonaqueous Sol–Gel Routes to Metal Oxide Nanoparticles. *Acc. Chem. Res.* **2007,** *40* (9), 793-800.

46. Bhakta, S.; Dixit, C. K.; Bist, I.; Jalil, K. A.; Suib, S. L.; Rusling, J. F., Sodium hydroxide catalyzed monodispersed high surface area silica nanoparticles. *Mater. Res. Express* **2016,** *3* (7), 075025.

47. Van Blaaderen, A.; Van Geest, J.; Vrij, A., Monodisperse colloidal silica spheres from tetraalkoxysilanes: Particle formation and growth mechanism. *J. Colloid Interface Sci.* **1992,** *154* (2), 481-501.

48. Liz-Marzán, L. M.; Giersig, M.; Mulvaney, P., Synthesis of Nanosized Gold−Silica Core−Shell Particles. *Langmuir* **1996,** *12* (18), 4329-4335.

49. Cichos, J.; Karbowiak, M., A general and versatile procedure for coating of hydrophobic nanocrystals with a thin silica layer enabling facile biofunctionalization and dye incorporation. *J. Mater. Chem. B* **2014,** *2* (5), 556-568.

50. Giesche, H., Synthesis of monodispersed silica powders II. Controlled growth reaction and continuous production process. *J. Eur. Ceram. Soc.* **1994,** *14* (3), 205-214.

51. Mine, E.; Yamada, A.; Kobayashi, Y.; Konno, M.; Liz-Marzán, L. M., Direct coating of gold nanoparticles with silica by a seeded polymerization technique. *J. Colloid Interface Sci.* **2003,** *264* (2), 385-390.

52. Gao, Y.; Wang, S.; Luo, H.; Dai, L.; Cao, C.; Liu, Y.; Chen, Z.; Kanehira, M., Enhanced chemical stability of VO_2 nanoparticles by the formation of SiO_2/VO_2 core/shell structures and the application to transparent and flexible VO_2-based composite foils with excellent thermochromic properties for solar heat control. *Energy Environ. Sci.* **2012,** *5* (3), 6104-6110.

53. Pastoriza-Santos, I.; Pérez-Juste, J.; Liz-Marzán, L. M., Silica-Coating and Hydrophobation of CTAB-Stabilized Gold Nanorods. *Chem. Mater.* **2006,** *18* (10), 2465-2467.

54. Westcott, S. L.; Oldenburg, S. J.; Lee, T. R.; Halas, N. J., Formation and Adsorption of Clusters of Gold Nanoparticles onto Functionalized Silica Nanoparticle Surfaces. *Langmuir* **1998,** *14* (19), 5396-5401.

55. Dong, A.; Ye, X.; Chen, J.; Kang, Y.; Gordon, T.; Kikkawa, J. M.; Murray, C. B., A Generalized Ligand-Exchange Strategy Enabling Sequential Surface Functionalization of Colloidal Nanocrystals. *J. Am. Chem. Soc.* **2011,** *133* (4), 998-1006.

56. Schick, I.; Lorenz, S.; Gehrig, D.; Schilmann, A.-M.; Bauer, H.; Panthöfer, M.; Fischer, K.; Strand, D.; Laquai, F.; Tremel, W., Multifunctional Two-Photon Active Silica-Coated Au@MnO Janus Particles for Selective Dual Functionalization and Imaging. *J. Am. Chem. Soc.* **2014,** *136* (6), 2473-2483.

57. Griffiths, C. H.; Eastwood, H. K., Influence of stoichiometry on the metal-semiconductor transition in vanadium dioxide. *J. Appl. Phys.* **1974**, 45 (5), 2201-2206.

58. McCafferty, E.; Wightman, J. P., An X-ray photoelectron spectroscopy sputter profile study of the native air-formed oxide film on titanium. *Appl. Surf. Sci.* **1999,** *143* (1), 92-100.

59. Morita, M.; Ohmi, T.; Hasegawa, E.; Kawakami, M.; Suma, K., Control factor of native oxide growth on silicon in air or in ultrapure water. *Appl. Phys. Lett.* **1989,** *55* (6), 562-564.

60. Luo, Y.-R., Bond Dissociation Energies. In *CRC Handbook of Chemistry and Physics*, 89th ed.; CRC Press/Taylor and Francis: Boca Raton, FL, 2009.

61. Israelachvili, J. N., Intermolecular and Surface Forces, 3rd ed.; Elsevier Inc., 2011.

62. Teng, Y.; Pong, P. W. T., One-Pot Synthesis and Surface Modification of Lauric-Acid-Capped $CoFe_2O_4$ Nanoparticles. *IEEE Trans. on Magn*. **2018**, 54 (11), 1-5.

63. Schladt, T. D.; Koll, K.; Prüfer, S.; Bauer, H.; Natalio, F.; Dumele, O.; Raidoo, R.; Weber, S.; Wolfrum, U.; Schreiber, L. M.; Radsak, M. P.; Schild, H.; Tremel, W., Multifunctional superparamagnetic MnO@SiO2 core/shell nanoparticles and their application for optical and magnetic resonance imaging. *J. Mater. Chem.* **2012**, 22, 9253-9262.

64. Mikolajczyk, A.; Gajewicz, A.; Rasulev, B.; Schaeublin, N.; Maurer-Gardner, E.; Hussain, S.; Leszczynski, J.; Puzyn, T., Zeta Potential for Metal Oxide Nanoparticles: A Predictive Model Developed by a Nano-Quantitative Structure–Property Relationship Approach. *Chem. Mater.* **2015**, 27 (7), 2400-2407.

65. Andrade, A. L.; Souza, D. M.; Pereira, M. C.; Fabris, J. D.; Domingues, R. Z., Synthesis and characterization of magnetic nanoparticles coated with silica through a sol-gel approach. *Cerâmica*. **2009**, 55 (336), 420-424.

66. Wu, R.; Qu, J.; Chen, Y., Magnetic powder $MnO–Fe_2O_3$ composite—a novel material for the removal of azo-dye from water. *Water Res.* **2009**, 39 (4), 630-638.

67. Taira, S.; Kitajima, K.; Katayanagi, H.; Ichiishi, E.; Ichiyanagi, Y., Manganese oxide nanoparticle-assisted laser desorption/ionization mass spectrometry for medical applications. *Sci Technol Adv Mater*. **2009**, 10 (3), 034602.

68. Jaroenworaluck, A.; Sunsaneeyametha, W.; Kosachan, N.; Stevens, R., Characteristics of silica-coated TiO_2 and its UV absorption for sunscreen cosmetic applications. *Surf. Interface Anal*. **2006**, 38 (4) , 474-477.

69. Trotman-Dickenson, A.F., Comprehensive Inorganic Chemistry (Ed.), Vol 3.; Pergamon Press: United Kingdom, 1973.